

# 光学学报

## 完美 Lommel 光束的产生

杨婧羽<sup>1</sup>, 周润<sup>1,2</sup>, 陈日坚<sup>1</sup>, 弓宁<sup>1</sup>, 范长江<sup>1</sup>, 任志君<sup>1\*</sup>

<sup>1</sup>浙江师范大学浙江省光信息检测与显示技术研究重点实验室, 浙江 金华 321004;

<sup>2</sup>义乌工商职业技术学院, 浙江 义乌 322000

**摘要** 引入了一种新型完美涡旋光束——完美 Lommel 光束 (PLBs)。首先给出了产生这种光束的理论机制, 然后构建实验系统来产生 PLBs。实验主要分为两步: 第一步是利用罗曼迂回相位编码法产生高质量 Lommel 光束; 第二步是将生成的 Lommel 光束经傅里叶变换后产生 PLBs。产生的 PLBs 的环半径不受拓扑荷值的影响, 并可通过阶数、不对称参数的模和角度三个参数来调控 PLBs 的分布, 这意味着 PLBs 是一种具有三个自由度的三参量完美涡旋光束。

**关键词** 物理光学; 完美 Lommel 光束; 罗曼迂回相位编码法; 复振幅调制

中图分类号 O436 文献标志码 A

DOI: 10.3788/AOS221096

### 1 引言

无衍射光束是一种在自由空间传播时具有空间不扩散性的光束。自从 Durnin 等<sup>[1]</sup>的开创性工作开展之后, 无衍射光束就引起了人们的广泛关注。除了经典的零阶贝塞尔光束<sup>[2]</sup>, 人们还相继提出并产生了其他无衍射光束, 包括涡旋光束<sup>[3-4]</sup>、艾里光束等<sup>[5-6]</sup>, 这类光束的光学形态仅由阶数控制, 因此属于单参量无衍射光束。后来, 研究者还引入并产生了具有复杂光学形态的双参量无衍射光束, 如马蒂厄光束<sup>[7]</sup>、抛物光束<sup>[8]</sup>等。

2014 年, Kotlyar 等<sup>[9-10]</sup>先后提出了几种非傍轴三参量无衍射光束, 主要包括非对称贝塞尔光束和可以用 Lommel 函数描述的 Lommel 光束<sup>[11]</sup>。除了阶数  $n$ , 还可以通过复数  $c = c_0 \exp(i\phi_0)$  来方便地调整 Lommel 光束的光场分布, 其中  $c$  是用来描述光束形态非中心对称分布的不对称参数,  $\phi_0$  是旋转角度, 模  $c_0$  取小于单位 1 的值, 以保证级数的收敛。与单参量和双参量的无衍射光束相比, 无衍射 Lommel 光束具有  $n$ 、 $c_0$ 、 $\phi_0$  三个调制参数, 因而是一种三参量无衍射光束。此外, Lommel 光束的显著优势还在于其分数阶轨道角动量 (OAM) 和它们光学形态之间的正交性<sup>[12]</sup>, 这无

疑为将 Lommel 光束应用于光通信领域、增加信息编码自由度提供了可能<sup>[13-15]</sup>。

在高质量产生无衍射 Lommel 光束的基础上, 本文引入并生成了一类三参量完美 Lommel 光束 (PLBs)。众所周知, 完美涡旋光束具有一个大小稳定的环形涡旋结构, 即环的大小与拓扑荷值无关。目前产生的完美光束主要包括经典的完美涡旋光束<sup>[16-17]</sup>、完美椭圆涡旋光束<sup>[18-19]</sup>以及其他类型的完美涡旋光束<sup>[20-22]</sup>。本文引入并产生的 PLBs 为完美光束增添了新的类型。

### 2 理论

在柱坐标系下, Lommel 函数在数学上可展开为一系列 Bessel 函数的叠加。因而无衍射 Lommel 光束的光场解析表达式<sup>[12]</sup>可以表示为

$$E_n(\rho, \phi, z) = \exp\left(iz\sqrt{k^2 - \alpha^2}\right) \sum_{p=0}^{\infty} (ic)^{2p} \exp\left[i(n + 2p)\phi\right] J_{n+2p}(\alpha\rho), \quad (1)$$

式中:  $\alpha$  是比例因子;  $\rho$ 、 $\phi$ 、 $z$  分别为径向、角向和轴向坐标;  $k$  为波数;  $J_{n+2p}$  为贝塞尔函数;  $p$  为整数; 复数  $c$  可以表示为  $c = c_0 \exp(i\phi_0)$ , 其中  $c_0$  取小于 1 的非负值, 旋转角度  $\phi_0$  的取值为  $(0, 2\pi)$ 。

柱坐标下 Lommel 光束的傅里叶变换可以写成

$$E(r, \theta, z) = \frac{k}{i2\pi f} \exp\left(iz\sqrt{k^2 - \alpha^2}\right) \times \int_0^{\infty} \int_0^{2\pi} \sum_{p=0}^{\infty} (ic)^{2p} \exp\left[i(n + 2p)\phi\right] J_{n+2p}(\alpha\rho) \times \exp\left[\frac{-ik}{f} \rho r \cos(\phi - \theta)\right] \rho d\rho d\phi = \frac{k}{i2\pi f} \exp\left(iz\sqrt{k^2 - \alpha^2}\right) \int_0^{\infty} \sum_{p=0}^{\infty} (ic)^{2p} J_{n+2p}(\alpha\rho) \rho d\rho \times \int_0^{2\pi} \exp\left[i(n + 2p)\phi\right] \exp\left[\frac{-ik}{f} \rho r \cos(\phi - \theta)\right] d\phi, \quad (2)$$

收稿日期: 2022-05-10; 修回日期: 2022-06-05; 录用日期: 2022-07-11; 网络首发日期: 2022-07-21

基金项目: 国家自然科学基金(11974314)

通信作者: \*renzhijun@zjnu.cn

式中:  $r, \theta$  分别为场源的径向、角向坐标;  $f$  是傅里叶变换透镜的焦距。

在推导式(2)时, 运用了下面的 Hankel 变换<sup>[23-24]</sup>:

$$\int_0^{2\pi} \exp\left[-ik\frac{r}{f}\rho \cos(\phi - \theta) + i(n + 2p)\phi\right] d\phi = 2\pi(-i)^{n+2p} \exp\left[i(n + 2p)\phi\right] J_{n+2p}\left(k\frac{r}{f}\rho\right), \quad (3)$$

所以根据式(2), 有

$$E(r, \theta, z) = \frac{k}{i2\pi f} \exp\left(iz\sqrt{k^2 - \alpha^2}\right) \int_0^{\infty} \sum_{p=0}^{\infty} (ic)^{2p} J_{n+2p}(\alpha\rho) \rho d\rho \times 2\pi(-i)^{n+2p} \exp\left[i(n + 2p)\phi\right] J_{n+2p}\left(k\frac{r}{f}\rho\right). \quad (4)$$

根据贝塞尔函数的正交性, 有

$$\alpha \int_0^{\infty} J_n(\alpha r) J_n\left(\frac{k\rho r}{f}\right) r dr = \delta\left(\alpha - \frac{k\rho}{f}\right), \quad (5)$$

式中:  $\delta$  为狄拉克函数。因此, 可以将式(5)化简为

$$E_n(r, \theta, z) = \frac{k}{\alpha f} \exp\left(iz\sqrt{k^2 - \alpha^2}\right) \delta\left(\alpha - \frac{kr}{f}\right) \times \sum_{p=0}^{\infty} (-i)^{n+2p} i^{2p-1} c^{2p} \exp\left[i(n + 2p)\theta\right], \quad (6)$$

显然, 式(6)是一种完美涡旋光束的表达式。将式(6)的光束命名为  $n$  阶 PLBs, 因为该光束的环半径与  $n$  无关, 这符合完美涡旋光束的特征<sup>[13]</sup>。根据式(6), 模拟了几种不同参数的 PLBs, 如图 1 所示。

图 1 表明, PLBs 的特征是在暗核的周围有两个不连续的对面对面弧形环。当拓扑荷值变化时, PLBs 环的半径保持不变, 这与经典的完美涡旋光束一致。复系数  $c$  是决定 PLBs 形状的一个重要参数,  $c$  的绝对值决定了弧长的大小。当  $|c|$  趋于 0 时, PLBs 的两个弧完全连接, 即  $n$  阶 PLBs 退化为经典的  $n$  阶完美涡旋光束。

理论上, 当  $|c|=0$  时, 式(1)可以写成

$$E(\rho, \theta) = \delta\left(\alpha - \frac{kr}{f}\right) \exp(im\theta), \quad (7)$$

式中:  $m$  为阶数。式(7)为经典完美涡旋光束的表达式<sup>[25]</sup>。随着  $|c|$  的增加, 弧长逐渐变短, 此外随着  $\phi_0$  的变化, PLBs 的弧也会相应地旋转。显然,  $|c|$  和  $\phi_0$  两个参数可以同时调控 PLBs 的分布形态。

为了产生 PLBs, 需要构建相应的实验系统。产生 PLBs 的前提是先产生高质量的 Lommel 光束。然而, 这在实验中并不容易实现。三参数 Lommel 光束是一种结构复杂的无衍射光束, Lommel 光束需要复振幅调制。但到目前为止, 仍没有一种商用光学元件能够同时调节光场的振幅和相位。过去 Zhao 等<sup>[26]</sup> 利用二进制振幅掩模来生成 Lommel 光束, 该掩模利用超像素编码的方法直接编码 Lommel 光束的复振幅信息。本文方案采用了计算全息法将相位和振幅信息同时编码到一块调制元件, 通过调制获得理想复振幅分布, 以产生 Lommel 光束。下面, 将介绍编码方法以及调制

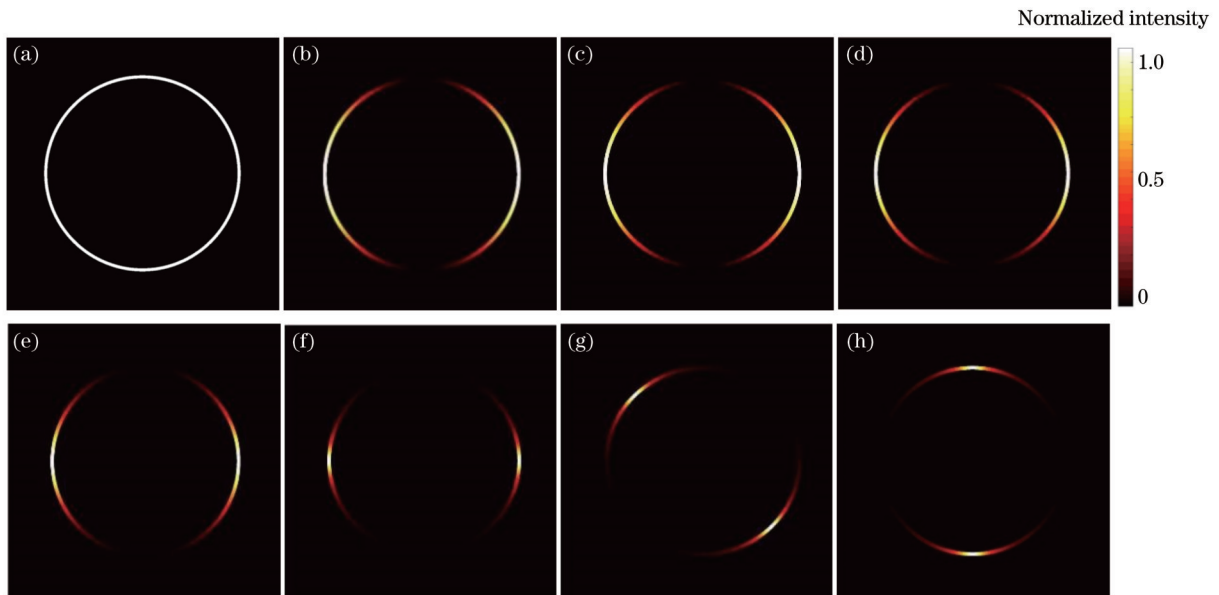


图 1 不同参数下 PLBs 的数值模拟图。(a)  $n=5, c_0=0, \phi_0=0$ ; (b)  $n=5, c_0=0.1, \phi_0=0$ ; (c)  $n=5, c_0=0.3, \phi_0=0$ ; (d)  $n=5, c_0=0.5, \phi_0=0$ ; (e)  $n=5, c_0=0.7, \phi_0=0$ ; (f)  $n=5, c_0=0.9, \phi_0=0$ ; (g)  $n=5, c_0=0.9, \phi_0=\pi/4$ ; (h)  $n=5, c_0=0.9, \phi_0=\pi/2$

Fig. 1 Numerical simulation diagrams of PLBs with different parameters. (a)  $n=5, c_0=0, \phi_0=0$ ; (b)  $n=5, c_0=0.1, \phi_0=0$ ; (c)  $n=5, c_0=0.3, \phi_0=0$ ; (d)  $n=5, c_0=0.5, \phi_0=0$ ; (e)  $n=5, c_0=0.7, \phi_0=0$ ; (f)  $n=5, c_0=0.9, \phi_0=0$ ; (g)  $n=5, c_0=0.9, \phi_0=\pi/4$ ; (h)  $n=5, c_0=0.9, \phi_0=\pi/2$

元件的制作。

### 3 计算全息法产生 Lommel 光束

基于光栅的衍射效应,基于罗曼迂回相位编码原理对光场复振幅进行编码。当平面波垂直入射等距光栅时,一级衍射为平面波。当局部光栅的栅距发生变化时,相应的相位会在某个衍射方向上发生超前或延迟,因此可以称之为迂回相位。显然,通过改变局部光栅栅距可以得到光束复振幅分布的相位调制,最后得到了所需的迂回相位二元计算全息图<sup>[27]</sup>。

将式(1)中 Lommel 光束的复振幅分解为振幅分布  $|A(r, \phi)|$  与相位分布  $\Phi(r, \phi) = \arg [A(r, \phi)]$ 。利用罗曼迂回相位编码方法,在全息图的所有采样单元

中打开一个矩形孔径。通过改变孔径的两个结构参数,即孔径的面积和孔径中心到采样中心的距离,实现复杂波前的振幅和相位调制。

图 2 为构造二元计算全息图(CGH)的算法步骤,利用该算法设计了生成几种 5 阶 Lommel 光束的二元计算全息图。图 3(a)、(d)、(g)、(j)为振幅分布图,图 3(b)、(e)、(h)、(k)为相位分布图,图 3(c)、(f)、(i)、(l)为编码后的二元计算全息图,图像大小为 35000 pixel×35000 pixel。为将设计好的二元计算全息图加工为全息掩模板,首先用图片分割软件将全息图分割成全息打印机能够识别的一系列 600 pixel×600 pixel 的小像素图片,然后将分割好的图片依次加载到全息打印机,在天津-III 型银盐干板曝光后,再经显影、定影处理得到所需掩模板。

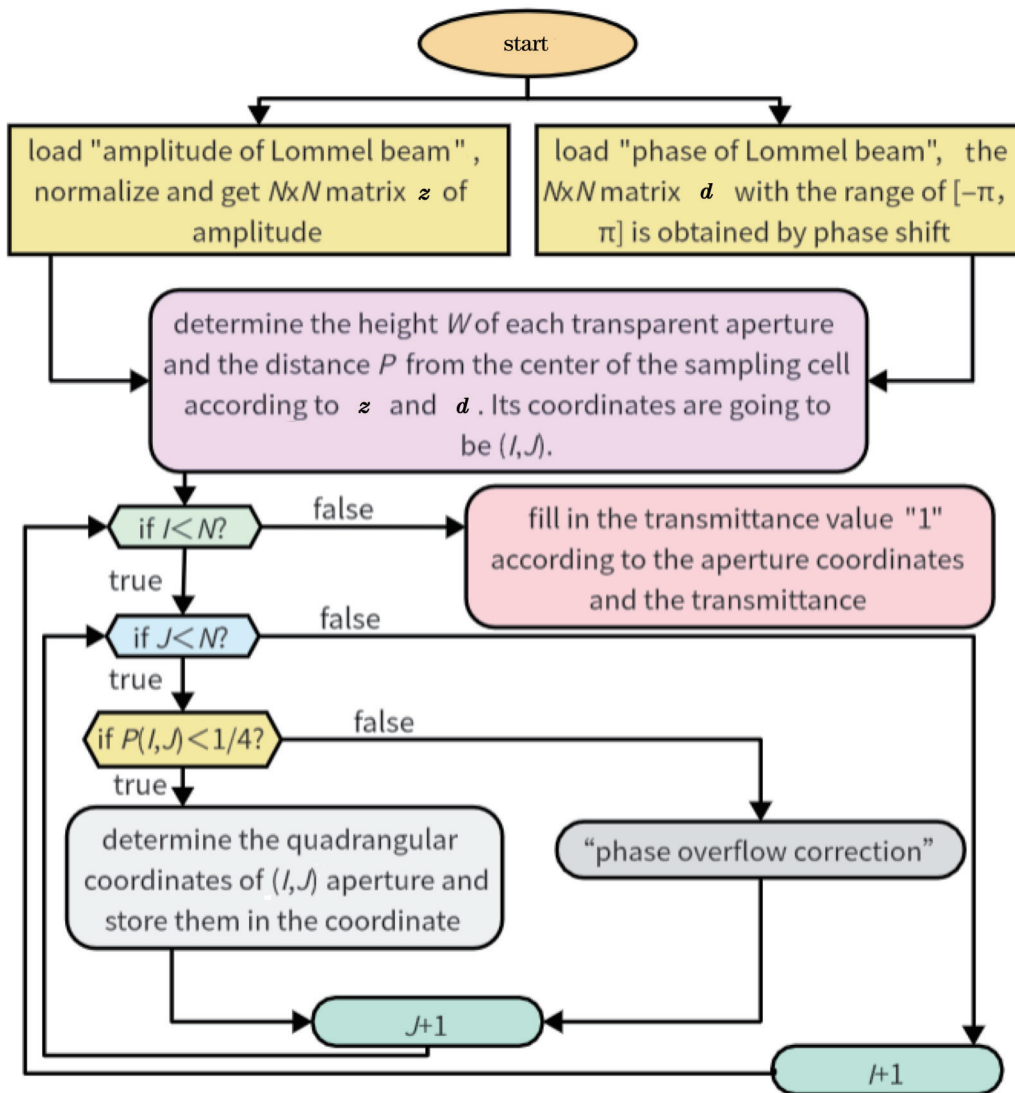


图 2 构建 PLBs 二元计算全息图的流程图

Fig. 2 Flow chart of constructing binary CGH of PLBs

### 4 实验产生 PLBs

产生 PLBs 的实验装置如图 4 所示,该实验光路由

两个关键部分组成,分别是 Lommel 光束的产生和 PLBs 的产生。在实验系统中,将经过 He-Ne 激光器的光束进行扩展和准直,将平面波入射到二元振幅计算

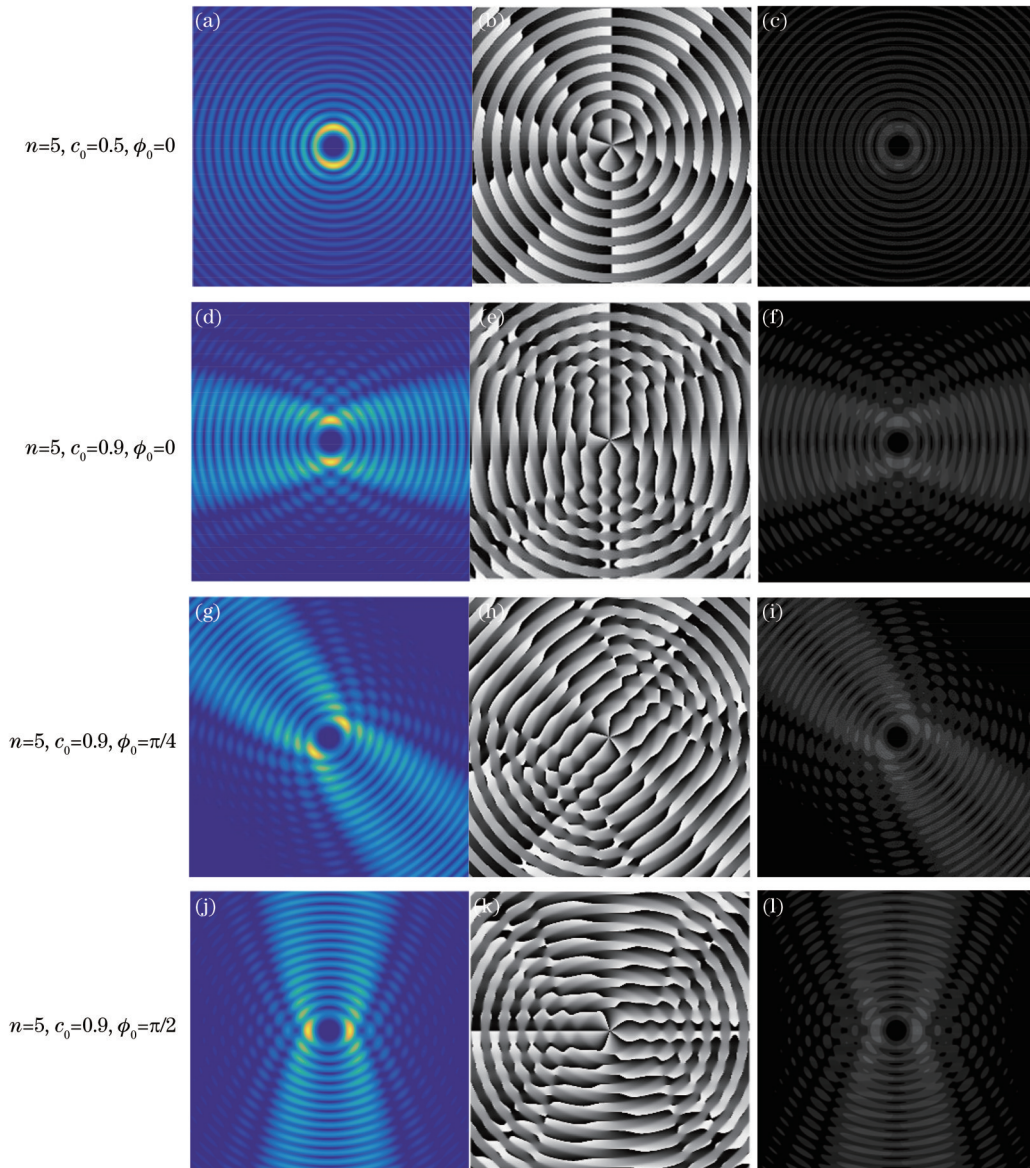


图 3 Lommel 光束的振幅分布图、相位分布图以及二元计算全息图。(a)(d)(g)(j)振幅分布图;(b)(e)(h)(k)相位分布图;(c)(f)(i)(l)二元计算全息图

Fig. 3 Amplitude distributions and phase distributions of Lommel beam and calculated binary CGHs. (a)(d)(g)(j) Amplitude distributions; (b)(e)(h)(k) phase distributions; (c)(f)(i)(l) calculated binary CGHs

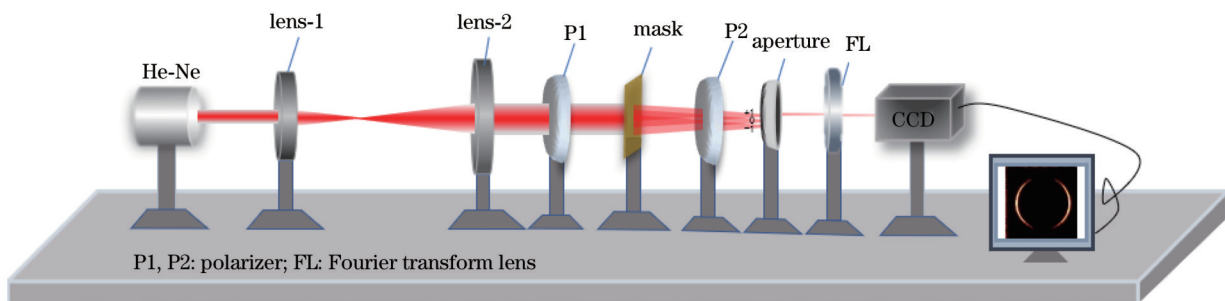


图 4 产生 PLBs 光束的实验光路图

Fig. 4 Experimental optical path of generating PLBs

全息图上,其中光束经扩展后直径约为 2 cm。计算全息图后用一个孔径作为滤光片,阻挡第 0 和 -1 级衍射光,使 +1 级衍射光通过。之后,生成的 Lommel 光束通过焦距为 30 cm 的傅里叶透镜,直接在透镜的后焦

平面上生成了 PLBs, 用 CCD (Flare 4M180-CL) 采集的实验图像如图 5 所示。实验结果与模拟结果(图 1)

吻合得较好。

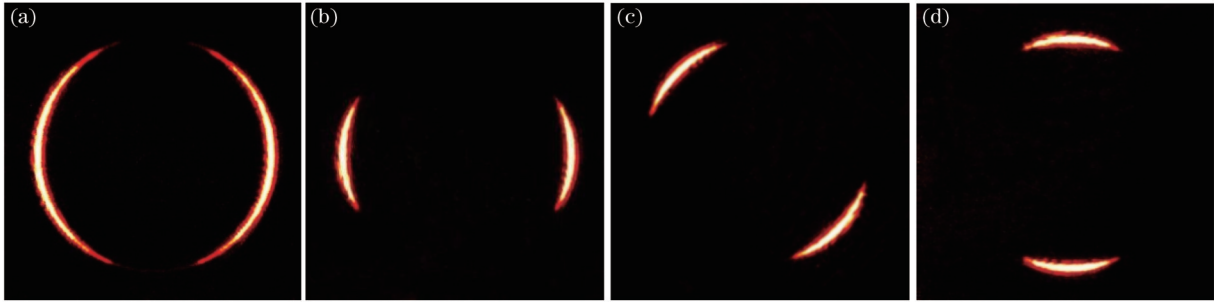


图 5 实验产生的 PLBs 光束。(a)  $n=5, c_0=0.5, \phi_0=0$ ; (b)  $n=5, c_0=0.9, \phi_0=0$ ; (c)  $n=5, c_0=0.9, \phi_0=\pi/4$ ; (d)  $n=5, c_0=0.9, \phi_0=\pi/2$

Fig. 5 Experimentally generated PLBs. (a)  $n=5, c_0=0.5, \phi_0=0$ ; (b)  $n=5, c_0=0.9, \phi_0=0$ ; (c)  $n=5, c_0=0.9, \phi_0=\pi/4$ ; (d)  $n=5, c_0=0.9, \phi_0=\pi/2$

## 5 PLBs 的轨道角动量

对于完美涡旋光束, 轨道角动量是它的一种重要

光学性质。这里将对 PLBs 的轨道角动量进行解析研究。

PLBs 的共轭复振幅为

$$E^*(r, \theta) = \delta\left(\alpha - \frac{kr}{f}\right) \sum_{p=0}^{\infty} i^{n+2p} (-i)^{2p-1} (c^*)^{2p} \left\{ \cos[(n+2p)\theta] - i \sin[(n+2p)\theta] \right\}, \quad (8)$$

式中:  $c^*$  为不对称参数  $c$  的共轭。PLBs 振幅的导数表达式为

$$\frac{\partial E}{\partial \theta} = \sum_{p=0}^{\infty} (-i)^{n+2p} i^{2p-1} c^{2p} \left\{ -(n+2p) \sin[(n+2p)\theta] + i(n+2p) \cos[(n+2p)\theta] \right\} \delta\left(\alpha - \frac{kr}{f}\right). \quad (9)$$

投影  $J_z$  的表达式为

$$J_z = \text{Im} \left( \int_0^R \int_0^{2\pi} E^* \frac{\partial E}{\partial \theta} r dr d\theta \right) = \lim_{R \rightarrow \infty} \sum_{p=0}^{\infty} (n+2p) \left\{ (c^*)^{2p} c^{2p} \int_0^{2\pi} \cos^2[(n+2p)\theta] d\theta - (c^*)^{2p} c^{2p} \int_0^{2\pi} \sin^2[(n+2p)\theta] d\theta \right\} \int_0^R \delta\left(\alpha - \frac{kr}{f}\right) \delta\left(\alpha - \frac{kr}{f}\right) r dr = 2\pi \lim_{R \rightarrow \infty} \sum_{p=0}^{\infty} (n+2p) (cc^*)^{2p} \int_0^R \delta^2\left(\alpha - \frac{kr}{f}\right) r dr, \quad (10)$$

式中:  $r$  为场源的径向坐标;  $\text{Im}(\cdot)$  表示复数的虚部。PLBs 的总横向强度  $I$  为

$$I = \int_0^R \int_0^{2\pi} E^* E r dr d\theta = \lim_{R \rightarrow \infty} \sum_{p=0}^{\infty} \left\{ (c^*)^{2p} c^{2p} \int_0^{2\pi} \sin^2[(n+2p)\theta] d\theta + (c^*)^{2p} c^{2p} \int_0^{2\pi} \cos^2[(n+2p)\theta] d\theta \right\} \int_0^R \delta\left(\alpha - \frac{kr}{f}\right) \delta\left(\alpha - \frac{kr}{f}\right) r dr = 2\pi \lim_{R \rightarrow \infty} \sum_{p=0}^{\infty} (cc^*)^{2p} \int_0^R \delta^2\left(\alpha - \frac{kr}{f}\right) r dr. \quad (11)$$

PLBs 的轨道角动量解析表达式为

$$\frac{J_z}{I} = \frac{\sum_{p=0}^{\infty} (cc^*)^{2p} (n+2p)}{\sum_{p=0}^{\infty} (cc^*)^{2p}} = n + \frac{2|c|^4}{1-|c|^4}. \quad (12)$$

由式(12)可知, PLBs 的轨道角动量与  $n$  和  $c_0$  两个参数有关, 而与  $\phi_0$  无关, 说明旋转的 PLBs 不改变轨道角动量。由  $c_0 < 1$ , 式(12)表明 PLBs 的轨道角动量是分数阶的, 这与经典完美涡旋的整数阶轨道角动量不同。分数阶轨道角动量光束在量子信息<sup>[28]</sup>、奇点光学<sup>[29]</sup>、宽带和光通信<sup>[30]</sup>等领域中有着重要作用。根据式(12), 绘制了 5 阶 PLBs 的轨道角动量与模  $c_0$  的关

系, 发现随着不对称参数模  $c_0$  的增加, 轨道角动量也增加(图 6)。涡旋光束的轨道角动量正是螺旋相位  $\exp[i(n+2p)\theta]$  的阶次  $n+2p$ 。由式(6)中 PLBs 的表达式也不难理解,  $c_0$  越大, 高阶螺旋相位  $\exp[i(n+2p)\theta]$  的权重系数越大, 因而叠加后对应的 PLBs 光束有更大的轨道角动量。

## 6 结 论

引入了一种由三个参数控制的三自由度完美涡旋光束——PLBs。为了产生这种 PLBs, 首先利用基于罗曼迂回相位编码法设计了一种二元计算全息图来产生高质量的 Lommel 光束。通过对 Lommel 光束进行

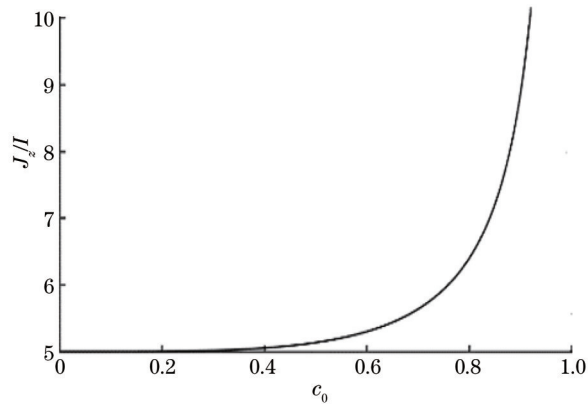


图 6 5阶PLBs的轨道角动量与 $c_0$ 的关系

Fig. 6 Relationship between orbital angular momentum and  $c_0$  of 5-order PLBs

傅里叶变换,得到了具有通用模态的PLBs。与传统的完美涡旋光束相比,生成的PLBs在空间光束振幅变形的控制方面具有很大的灵活性。此外,PLBs还具有分数阶轨道角动量。具有三个调制自由度的PLBs有更为丰富的光学形态,可在光通信、微操纵、量子信息编码等领域发挥独特的作用。

#### 参 考 文 献

- [1] Durnin J, Miceli J, Jr., Eberly J H. Diffraction-free beams[J]. *Physical Review Letters*, 1987, 58(15): 1499-1501.
- [2] 谢家俊, 唐诗瑶, 陈永强, 等. 贝塞尔光束在生物组织中的自重建特性研究[J]. *中国激光*, 2022, 49(5): 0507302.  
Xie J J, Tang S Y, Chen Y Q, et al. Self-reconstruction characteristics of Bessel beam in biological tissue[J]. *Chinese Journal of Lasers*, 2022, 49(5): 0507302.
- [3] Zhan Q W. Properties of circularly polarized vortex beams[J]. *Optics Letters*, 2006, 31(7): 867-869.
- [4] 罗蒙. 一种产生涡旋光束的勾型阵列超表面结构设计[J]. *激光与光电子学进展*, 2021, 58(1): 0108001.  
Luo M. Design of hook-typed metasurface for vortex beams generation[J]. *Laser & Optoelectronics Progress*, 2021, 58(1): 0108001.
- [5] Siviloglou G A, Broky J, Dogariu A, et al. Observation of accelerating Airy beams[J]. *Physical Review Letters*, 2007, 99(21): 213901.
- [6] 韩洪民, 范引鹏, 杨叶城, 等. 基于变形镜的多波长艾里光束生成与传播特性[J]. *光学学报*, 2021, 41(16): 1626001.  
Han H M, Fan Y P, Yang Y C, et al. Generation and propagation characteristics of multi-wavelength Airy beams based on deformable mirrors[J]. *Acta Optica Sinica*, 2021, 41(16): 1626001.
- [7] Gutiérrez-Vega J C, Iturbe-Castillo M D, Chávez-Cerda S. Alternative formulation for invariant optical fields: Mathieu beams[J]. *Optics Letters*, 2000, 25(20): 1493-1495.
- [8] Bandres M A, Gutiérrez-Vega J C, Chávez-Cerda S. Parabolic nondiffracting optical wave fields[J]. *Optics Letters*, 2004, 29(1): 44-46.
- [9] Kotlyar V V, Kovalev A A, Soifer V A. Asymmetric Bessel modes[J]. *Optics Letters*, 2014, 39(8): 2395-2398.
- [10] Kotlyar V V, Kovalev A A, Skidanov R V, et al. Asymmetric Bessel-Gauss beams[J]. *Journal of the Optical Society of America A, Optics, Image Science, and Vision*, 2014, 31(9): 1977-1983.
- [11] Kovalev A A, Kotlyar V V. Diffraction-free Lommel beams[J]. *Computer Optics*, 2014, 38(2): 188-192.
- [12] Kovalev A A, Kotlyar V V. Lommel modes[J]. *Optics Communications*, 2015, 338: 117-122.
- [13] Li Y, Zhang Y X, Zhu Y. Lommel-Gaussian pulsed beams carrying orbital angular momentum propagation in asymmetric oceanic turbulence[J]. *IEEE Photonics Journal*, 2020, 12(1): 7900915.
- [14] Wang S L, Yang D H, Zhu Y, et al. Capacity analysis of oceanic channels with localized Lommel-Gaussian vortex beams [J]. *Applied Optics*, 2021, 60(14): 4135-4142.
- [15] Lu Z H, Yan B L, Chang K, et al. Space division multiplexing technology based on transverse wavenumber of Lommel-Gaussian beam[J]. *Optics Communications*, 2021, 488: 126835.
- [16] Ostrovsky A S, Rickenstorff-Parrao C, Arrizón V. Generation of the "perfect" optical vortex using a liquid-crystal spatial light modulator[J]. *Optics Letters*, 2013, 38(4): 534-536.
- [17] Vaity P, Rusch L. Perfect vortex beam: Fourier transformation of a Bessel beam[J]. *Optics Letters*, 2015, 40(4): 597-600.
- [18] Li L, Chang C L, Yuan C J, et al. High efficiency generation of tunable ellipse perfect vector beams[J]. *Photonics Research*, 2018, 6(12): 1116-1123.
- [19] Li D L, Chang C L, Nie S P, et al. Generation of elliptic perfect optical vortex and elliptic perfect vector beam by modulating the dynamic and geometric phase[J]. *Applied Physics Letters*, 2018, 113(12): 121101.
- [20] Wang H, Fu S Y, Gao C Q, et al. Tailoring a complex perfect optical vortex array with multiple selective degrees of freedom [J]. *Optics Express*, 2021, 29(7): 10811-10824.
- [21] Zhang H, Li X Z, Ma H X, et al. Grafted optical vortex with controllable orbital angular momentum distribution[J]. *Optics Express*, 2019, 27(16): 22930-22938.
- [22] Li X X, Ren Z J, Xu F Y, et al. Generation of perfect helical Mathieu vortex beams[J]. *Optics Express*, 2021, 29(20): 32439-32452.
- [23] Friberg A T. Stationary-phase analysis of generalized axicons[J]. *Journal of the Optical Society of America A*, 1996, 13(4): 743-750.
- [24] Arlt J, Dholakia K. Generation of high-order Bessel beams by use of an axicon[J]. *Optics Communications*, 2000, 177(1/2/3/4/5/6): 297-301.
- [25] Kotlyar V V, Kovalev A A, Porfirev A P. Optimal phase element for generating a perfect optical vortex[J]. *Journal of the Optical Society of America A, Optics, Image Science, and Vision*, 2016, 33(12): 2376-2384.
- [26] Zhao Q, Gong L, Li Y M. Shaping diffraction-free Lommel beams with digital binary amplitude masks[J]. *Applied Optics*, 2015, 54(25): 7553-7558.
- [27] 苏显渝, 李继陶. 信息光学[M]. 北京: 科学出版社, 1999.  
Su X Y, Li J T. *Information optics*[M]. Beijing: Science Press, 1999.
- [28] Oemrawsingh S S R, Ma X, Voigt D, et al. Experimental demonstration of fractional orbital angular momentum entanglement of two photons[J]. *Physical Review Letters*, 2005, 95(24): 240501.
- [29] Volyar A, Bretsko M, Akimova Y, et al. Vortex avalanche in the perturbed singular beams[J]. *Journal of the Optical Society of America A, Optics, Image Science, and Vision*, 2019, 36(6): 1064-1071.
- [30] Kotlyar V V, Kovalev A A. Controlling orbital angular momentum of an optical vortex by varying its ellipticity[J]. *Optics Communications*, 2018, 410: 202-205.

## Production of Prefect Lommel Beams

Yang Jingyu<sup>1</sup>, Zhou Run<sup>1,2</sup>, Chen Rijian<sup>1</sup>, Gong Ning<sup>1</sup>, Fan Changjiang<sup>1</sup>, Ren Zhijun<sup>1\*</sup>

<sup>1</sup>Key Laboratory of Researching Optical Information Detecting and Display Technology in Zhejiang Province,

Zhejiang Normal University, Jinhua 321004, Zhejiang, China;

<sup>2</sup>Yiwu Industrial and Commercial College, Yiwu 322000, Zhejiang, China

### Abstract

**Objective** Non-diffractive beams have been widely researched since their birth. The Lommel beams are a kind of nondiffractive beams, which have a complex structure and can be described by Lommel functions. The optical morphology of the non-diffractive Lommel beams can be modulated by three parameters, i.e., the topological charge  $n$ , the asymmetry parameter  $c_0$ , and the rotation angle  $\phi_0$ . Apparently, Lommel beams differ from the one-parameter non-diffractive beams (Bessel beams, vortex beams, and Airy beams) and two-parameter non-diffractive beams (Mathieu beams and parabolic beams). The structure of three-parameter Lommel beams is more complex, and their optical morphology is more abundant than that of the one-parameter and two-parameter non-diffractive beams. For a traditional vortex beam, its structure is a bright ring around the middle dark core, and its topological charge affects the size of the bright ring radius. To solve this problem, researchers introduce the perfect vortex beam. The main optical property of the perfect vortex beam is that it has a ring vortex structure with stable size, namely that the size of the ring is independent of the topological charge. At present, perfect vortex beams mainly include classical perfect vortex beams and perfect elliptical vortex beams. This study attempts to produce perfect beams with more abundant optical morphology. In other words, we hope to generate perfect Lommel beams (PLBs) on the basis of diffraction-free Lommel beams, and the optical morphology of the produced PLBs can be adjusted by the three parameters at the same time.

**Methods** Classical perfect beams are generated through the Fourier transform of Bessel beams. In this paper, we use the Fourier transform of Lommel beams to generate a new kind of perfect beams, i.e., PLBs. Complex amplitude modulation, namely that the amplitude and phase of beams are modulated simultaneously, is necessary for the generation of Lommel beams with a complex structure. It is easy to construct the amplitude modulation and phase modulation elements separately for beam generation, but the accurate alignment of the two elements is difficult. To produce high-quality Lommel beams, we need to introduce an encoding method to construct the complex amplitude modulation element, where the main purpose of encoding is to encode the amplitude and phase information of wavefront in one modulation element. Generally speaking, amplitude modulation is relatively easy. We adopt the Lohmann-type detour phase encoding method to modulate the complex amplitude of beams, which uses the diffraction effect of irregular grating, and by changing the grid spacing of local grating, we can obtain the required phase information at a certain diffraction level. With this encoding method, we construct a binary computer-generated hologram (CGH) that can produce Lommel beams. In the hologram, we can realize the amplitude modulation of beams by opening a rectangular optical aperture in the sampling unit of the hologram. Moreover, we can also realize phase modulation of beams by changing the two structural parameters of the aperture, i.e., the area of the aperture and the distance between its center and the sampling center. Then, the obtained binary CGHs for generating Lommel beams are machined into a mask with high resolution and high pixel number by the homemade holographic direct-writing printing system. For mask machining, first, the designed photolithography file (i.e., hologram) is automatically divided into a series of unit patterns with 600 pixel $\times$ 600 pixel. These patterns are automatically input into a digital mirror device in accordance with their sequences and are scanned line by line for projection exposure on a Tianjin-III silver halide dry plate. When the lithography is completed, the silver halide dry plate is processed to obtain the amplitude mask. Finally, a high-quality Lommel beam is generated by the machined mask. On this basis, PLBs can be obtained by the Fourier transform of the generated Lommel beams.

**Results and Discussions** In cylindrical coordinates, the Lommel function can be mathematically expanded as the superposition of Bessel functions, and the expression of PLBs can be derived by the Fourier transform of the Lommel function. We can readily learn from the expression of PLBs that the ring radius of PLBs is independent of the order, which is consistent with the characteristics of perfect vortex beams. Then, we theoretically simulate several kinds of PLBs with different parameters (Fig. 1). Finally, PLBs are experimentally generated. By the Lohmann-type detour phase coding method, the amplitude and phase of the complex wavefront of Lommel beams are coded simultaneously. The algorithm steps for constructing a binary CGH are given in Fig. 2, and on the basis of the algorithm, the binary CGH for generating

Lommel beams is constructed (Fig. 3). The binary CGH of Lommel beams with other parameters can also be easily obtained by the same method proposed in this paper. We machine binary CGHs into binary amplitude masks by the holographic direct-writing printing system. The calculated CGHs are of 35000 pixel $\times$ 35000 pixel, with the size of a pixel of 318 nm $\times$ 318 nm, and hence the size of machined binary masks is 11.0 mm $\times$ 11.0 mm. We construct an experimental setup to generate PLBs by using the machined binary amplitude masks (Fig. 4). The +1 order diffraction of masks is filtered by a keyhole, and then by the Fourier transform of Lommel beams, the PLBs are obtained and recorded by a scientific CCD camera (Flare 4M180-CL) (Fig. 5). It can be observed that the generated PLBs are in good agreement with their theoretical results. In addition, the orbital angular momentum of the PLBs is studied analytically, and the relationship between orbital angular momentum and mode of the fifth-order PLBs is plotted (Fig. 6).

**Conclusions** We introduce and generate a type of new perfect vortex beams, i. e., PLBs. Firstly, the theoretical mechanisms of PLB generation are deduced. Then, the experimental generation system is constructed to generate PLBs. The experiment system is mainly divided into two parts. The first part is to generate high-quality Lommel beams by the Lohmann-type detour phase encoding method, and the second part is to generate PLBs by the Fourier transform of the generated Lommel beams. The ring radius of the generated PLBs is not dependent on the topological charge value, and the optical distribution of PLBs can be controlled by three parameters, namely, the order, modulus of asymmetric parameters, and angle. This means that PLBs are perfect vortex beams with three degrees of freedom.

**Key words** physical optics; perfect Lommel beams; Lohmann-type detour phase encoding method; complex amplitude modulation